Metallo-Dielectric Electromagnetic Bandgap Structures for Suppression and Isolation of the Parallel-Plate Noise in High-Speed Circuits

Ramesh Abhari, *Student Member, IEEE,* and George V. Eleftheriades, *Senior Member, IEEE*

***Abstract*—A novel approach for the suppression of the parallel-plate waveguide (PPW) noise in high-speed printed circuit boards is presented. In this approach, one of the two conductors forming the PPW is replaced by an electromagnetic bandgap (EBG) surface. The main advantage of the proposed approach over the commonly practiced methods is the omnidirectional noise suppression it provides. For this purpose, two EBG structures are initially designed by utilizing an approximate circuit model. Subsequently, the corresponding band structures are characterized by analytical solutions using the transverse resonance method, as well as full-wave finite-element simulations. The designed EBG surfaces were fabricated and employed in a number of PPW test boards. The corresponding frequency-domain measurements exhibited bandgaps of approximately 2.21 and 3.35 GHz in the frequency range below 6 GHz. More importantly, suppression of the PPW noise by 53% was achieved based on time-domain reflectometry experiments, while maintaining the signal transmission quality within the required specifications for common signaling standards.**

***Index Terms*—Electromagnetic bandgap (EBG) structures, ground/power noise, parallel-plate noise, periodic structures, suppression of the switching noise.**

I. Introduction

EXCITATION of the parallel-plate waveguide (PPW) mode is an artifact of conduction of a time-varying current through vias in parallel-plate environments [e.g., multilayer printed circuit boards (PCBs)]. In spite of its deterministic nature, this mode is referred to as noise with terms such as power/ground noise, ground bounce, simultaneous switching noise (SSN), etc. This noise can produce false switching in digital circuits and malfunctioning in analog circuits, which would eventually render them inoperable. With the ever-increasing clock frequencies of digital circuits, the bottleneck imposed by the power/ground noise becomes more and more significant. Therefore, both characterization and suppression of the PPW noise are deemed crucial in high-speed circuit design. The analysis of this type of noise has been the focus of many research works, which are referred to and categorized in [1]. On the other hand, in practice, different techniques are commonly used to suppress the parallel-plate noise, which are summarized as follows.

1) Adding discrete decoupling capacitors to provide a grounding path for the voltage fluctuations on the reference dc voltage planes [2].
2) Employing buried decoupling capacitors where parallel planes configure a distributed capacitor. In comparison with discrete capacitors, buried capacitors are less prone to parasitics and offer better performance at higher frequencies [3].
3) Selecting the location of the via ports in a manner that eliminates certain package resonances, thus leading to the reduction of the coupling between ports through the parallel-plate noise [4].
4) Employing differential interconnects, which inherently reject the common-mode noise [5].

The underlying common feature in describing the performance of all these methods is the localized suppression of the PPW noise they offer.

In this paper, a metallic electromagnetic bandgap (EBG) structure is proposed to function as a planar bandstop filter that blocks the RF noise currents throughout the power/ground planes. In fact, the term bandgap implicitly refers to an omnidirectional stopband, which is the desired characteristic for this type of application. EBG structures have been previously employed for suppressing unwanted RF surface currents in high-frequency analogue applications [6], [7]. In [6], uniplanar EBG structures have been utilized to suppress leakage in stripline circuits above 9 GHz. For this purpose, a two-dimensional (2-D) EBG was realized by etching a periodic slot pattern on both ground planes [6]. Unfortunately, the resulting perforated ground planes are prone to leakage through radiation, especially when operating within the bandgap [8].

The challenge in employing EBGs for the suppression of the parallel-plate noise in high-speed circuits arises due to the following two reasons: 1) a typical parallel-plate noise pattern has a low-pass spectrum ($<$ 6 GHz), thus requiring a compact low-frequency EBG structure and 2) the EBG should span enough bandwidth to effectively suppress the PPW noise. Suitable metallic EBG surfaces that satisfy these requirements and are not prone to radiation leakage, seem to be the structures proposed by Sievenpiper *et al.* for antenna applications [7].

Manuscript received October 10, 2002; revised January 27, 2003. This work was supported by the Government of Ontario and by the Centre for Manufacturing Assembly and Packaging, University of Toronto.

The authors are with The Edward S. Rogers Sr. Department of Electrical and Computer Engineering, University of Toronto, Toronto, ON, Canada M5S 3G4 (e-mail: ramesh@waves.utoronto.ca; gelefth@waves.utoronto.ca).

Digital Object Identifier 10.1109/TMTT.2003.812555

The current study, documented here and in an earlier conference publication by the authors [9], is the first report on the application of an EBG surface for the suppression of the parallel-plate noise in high-speed digital circuits. In this paper, the proposed approach, which was briefly introduced in [9], is elaborated and different methods for the prediction of the key feature, i.e., the bandgap characteristics of an EBG surface in a PPW environment, are compared. As well, in order to improve the noise suppression, another EBG surface having a simpler geometry, but a wider bandgap compared to the structure of [9], is designed and fabricated. In addition, the transmission characteristics of a signal line in the presence of an EBG ground are characterized in the time domain.

The herein proposed approach is superior to the other PPW noise-suppression methods mentioned before because it provides a *global* solution as it blocks the PPW noise *all over* the parallel plates, i.e., *in all azimuthal* directions. Moreover, this method benefits from the *a priori* knowledge of the noise spectrum, which can be obtained in a cost-effective manner from circuit simulations [1], thus enabling the design of the noise-suppression EBG filter ahead of the manufacturing process. This is in contrast to the most common approach for the suppression of the PPW noise, i.e., the use of decoupling capacitors, where their performance is degraded due to the parasitics that emerge after fabrication.

The organization of this paper is as follows. In Section II, the spectrum of the PPW noise in a given structure is predicted by using the physics-based computer-aided design (CAD) model of [1]. Based on this information, two EBG surfaces are designed to create a relatively wide bandgap in the determined noise bandwidth. In Section III, the transverse resonance method (TRM) is employed to derive the dispersion relations and to generate the respective diagrams for these EBG structures when incorporated into a PPW arrangement. Subsequently, the predicted dispersion characteristics are verified not only with finite-element eigenmode simulations, but also through experiments on a number of test boards for insertion-loss measurements. In Section IV, the performance of the EBG surfaces for improving port isolation is investigated through time-domain reflectometry and frequency-domain measurements. Lastly, in Section V, the signal transmission on a stripline having one EBG ground is experimentally characterized.

II. Design of the EBG Structures

In order to achieve an efficient suppression of the PPW noise, two characteristics of the circuit should be identified, i.e., the noise margin and PPW noise spectrum. The former is one of the technological characteristics of the circuit given by the manufacturers, and the latter can be obtained from any of the various simulation methods for the prediction of the PPW noise, as described in [1].

For instance, consider the simple parallel-plate structure shown in Fig. 1. The physics-based CAD model for vias in parallel-plate environments, which was developed in [1], is utilized to predict the spectrum of the noise at Port 2 when Port 1 is excited by a 200-mV step voltage of 110-ps rise time. The

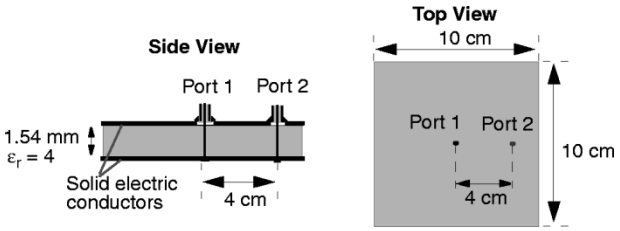

Fig. 1. Single-layer PPW structure.

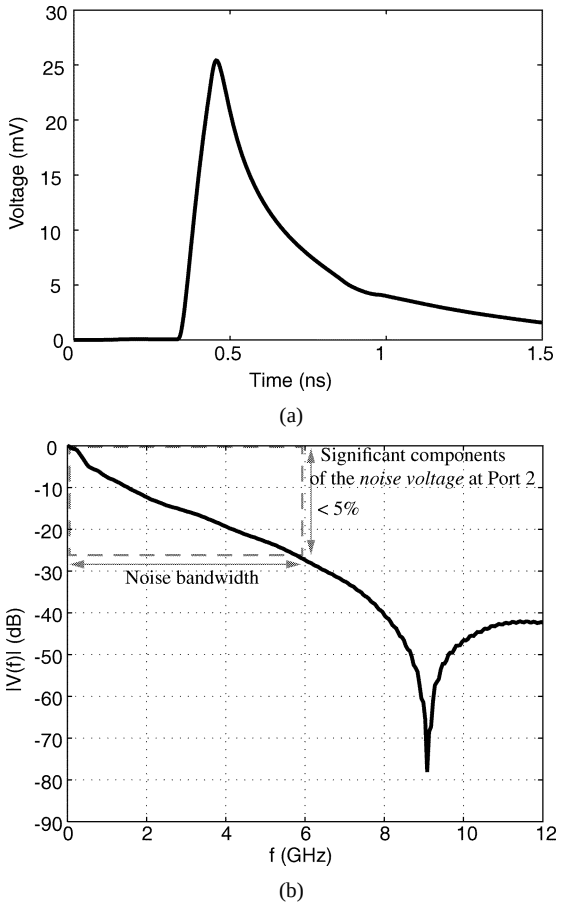

Fig. 2. (a) Time-domain signature of the noise probed at Port 2 of the structure shown in Fig. 1. (b) Normalized noise spectrum.

time-domain signature and the frequency-domain spectrum of the parallel-plate noise detected at Port 2 are presented in Fig. 2. It can be observed that the noise spectrum exhibits a low-pass characteristic. The noise bandwidth in Fig. 2 is defined to span the region from dc to 6 GHz where the magnitude of the frequency spectrum drops to 5% of its maximum. Hence, a planar wide-band bandstop filter designed to operate in this region can efficiently suppress the parallel-plate noise. The design and fabrication procedures of such bandstop filters are presented in the following sections.

A. Design Procedure

Due to the considerations discussed in Section I (such as the elimination of the back radiation and the achievement of compact geometries at low frequencies), the general class of the metallo-dielectric EBG structures proposed in [7] has been selected to realize the planar omnidirectional bandstop filter. Commonly,

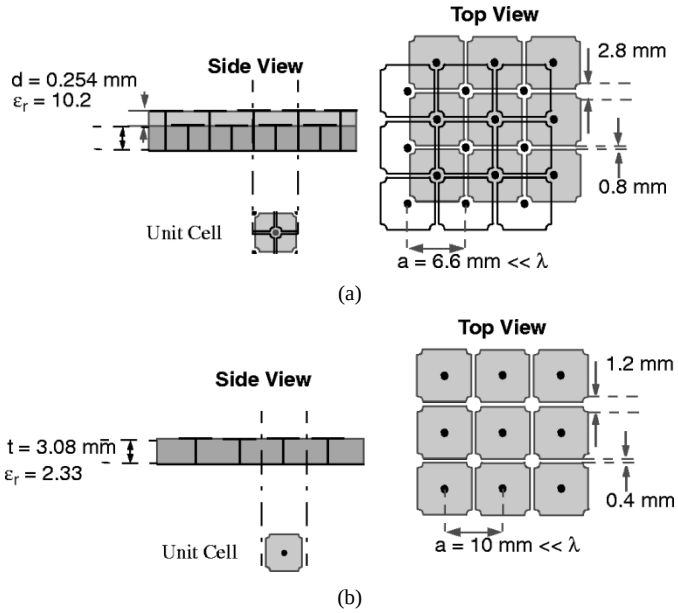

Fig. 3. Metallo-dielectric EBG structures. (a) Three layer. (b) Two layer.

these configurations contain two or three metal layers, as shown in Fig. 3, and are called two- and three-layer structures, respectively.

According to [7], as long as the wavelength is much longer than the size of the individual cells in these periodic structures, the surface impedance can be represented by an equivalent parallel resonant *L–C* circuit. The inductance *L* and capacitance *C* are the sheet inductance and sheet capacitance of the EBG structure, which can be determined by approximate closed-form relations given in [10] or by more accurate numerical field solutions. The relative bandwidth of this *L–C* resonator is proportional to $\sqrt{L/C}$. Therefore, for our intended wide-band application, the ratio of *L–C* should maintain a relatively large value in the design of the EBG structure. For the total elimination of the parallel-plate noise shown in Fig. 2, it is desired to have a 6-GHz bandgap, but in practice, this proves quite difficult to be achieved at the low gigahertz frequency range. It should be mentioned here that, in the stopband, the *L–C* resonator becomes an open circuit, therefore, the EBG surface can be considered as a magnetic wall. It can be shown that a parallel-plate configuration formed by a conductor and a magnetic wall does not support the TM_{00} mode, which is, in fact, the fundamental mode responsible for the PPW noise.

The design of this EBG structure is an iterative process consisting of the following proposed steps.

Step 1) Choose the resonance frequency of the *L–C* circuit by monitoring the noise spectrum through fast simulations utilizing the model developed in [1].

Step 2) Choose the values of *L* and *C* to achieve the resonance frequency of Step 1 while maintaining the *L–C* ratio relatively high to obtain a wide stopband.

Step 3) Calculate the dimensions of the unit cell of the EBG structure to achieve the values of *L* and *C* selected in Step 2.

Step 4) If the calculated dimensions are not realizable with available and cost-effective substrates, then start from step 1 with a slightly different resonance frequency.

Considering the manufacturing constraints and following the above recursive design procedure, reasonable values of L and C, which simultaneously meet the low-frequency, but wide-band resonance requirements, have been determined for the two EBG configurations shown in Fig. 3. The dimensions of their respective unit cells, i.e., the size of the patch and height of the via, as well as the spacing between the cells, have been derived using the closed-form expressions given in [10].

The geometries shown in Fig. 3 correspond to $L = 3.86$ nH/□ and $C = 0.67$ pF · □ for the two-layer structure, and $L = 2$ nH/□ and $C = 1.25$ pF · □ for the three-layer structure, which result in resonance frequencies of 3.13 and 3.18 GHz, respectively. These frequencies indeed lie around the center of the noise bandwidth in Fig. 2(b). Note that, in the calculation of the sheet inductance, the inductances due to the vias are not included.

B. Fabrication

Usually, in both types of two- and three-layer EBG structures, the bottom substrate is relatively thick to achieve a sheet inductance of a few nanohenrys/□. The sheet capacitance of the three-layer structures is higher than that of the two-layer structures because of the parallel-plate capacitor formed by the patches on the second and third metal layers. Therefore, the three-layer structure appears to be more suitable for achieving resonance frequencies below 5 GHz when typical FR4 laminates are employed. As a result, the structure shown in the Fig. 3(a) was initially fabricated and tested. A picture of the constructed EBG is presented in Fig. 4(a). In this embodiment, the bottom substrate is a double-sided FR4 board with periodic (almost square-shape) patches etched on the top metal surface. The top dielectric, with the higher dielectric constant, is a single-sided Rogers RT/Duroid 6010 laminate with the same square-shape patches on the conductor side. All the patches in the second and third metal layers are connected to the solid metal layer at the bottom by conducting vias. It should be mentioned that between the FR4 and the RT/Duroid laminate, there is no adhesive material, instead, a very thin layer of air exists, which lowers the effective dielectric constant between the patches.

The two-layer structure, which is shown in Fig. 3(b), has been fabricated using a thicker substrate, i.e., Rogers RT/Duroid 5870, to increase the sheet inductance and the bandwidth thereof. This laminate has a lower permittivity compared to FR4. In order to maintain the required value of the sheet capacitance for the target resonance frequency, the dimensions of the patches have been increased compared to those of the three-layer EBG, as can be seen in the picture of the fabricated structure shown in Fig. 4(b). In the same fashion as before, the patches on the top surface are connected to the bottom solid metal surface by conducting vias.

III. Predicting the Bandgap

Representing the EBG structure with a parallel *L–C* circuit does not fully predict the characteristics of the EBG structure, and only estimates an approximate resonance frequency. More

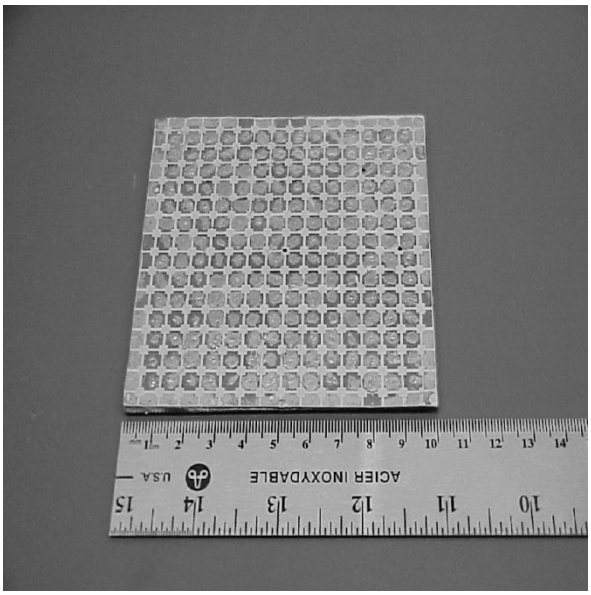

(a)

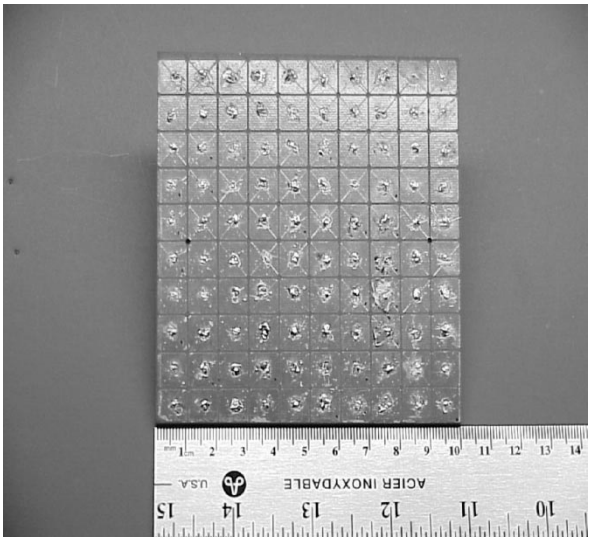

(b)

Fig. 4. Fabricated metallo-dielectric EBG structures. (a) Three layer. (b) Two layer.

importantly, in the applications discussed in this paper, the EBG surface is installed in a closed environment (i.e., a PPW), unlike the radiation into open-space applications examined in [7] and [10]. In order to predict the bandgap accurately, analytical solutions and full-wave numerical methods are investigated here for the parallel-plate configuration with an EBG surface.

A. Prediction of the Bandgap by Utilizing the TRM

The TRM is a well-established technique for finding the cutoff frequencies of waveguides with partial fillings or corrugated walls [11], [12]. This general method has been utilized to determine the dispersion characteristics of a PPW with an EBG surface replacing one of the conductor plates. In applying the resonance condition to the cross section of the PPW, the surface is represented by its equivalent parallel *L–C* circuit, as shown in Fig. 5.

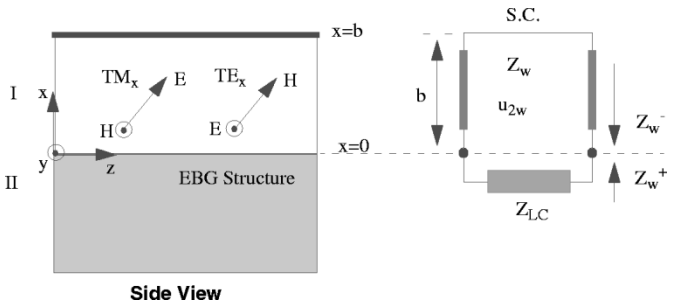

Fig. 5. Transverse resonance model for a PPW structure with one EBG surface.

Note that, in the resonant circuit representation of the surface, which was discussed in Section II, no component is included to account for the loading of the *L–C* circuit due to the environment above the surface such as free space or an additional plate. However, when the *L–C* circuit is combined with the TRM, this element is implicitly incorporated. As shown in Fig. 5, the wave impedance looking into the $x < 0$ direction is Z_{LC}. The wave impedance looking into the $x > 0$ direction can be simply derived by considering the top region as a short-circuited transmission line with a characteristic impedance Z_w. In fact, Z_w is the wave impedance determined by the type of mode being investigated, i.e., TM_x or TE_x.

$$Z_{x<0} = \frac{jL\omega}{1 - LC\omega^2} \tag{1a}$$

$$Z_{x>0}^{\mathrm{TM}} = -j\frac{u_2}{\omega\varepsilon}\tanh(u_2 b) \tag{1b}$$

$$Z_{x>0}^{\mathrm{TE}} = j\frac{\omega\mu}{u_2}\tanh(u_2 b) \tag{1c}$$

where $u_2^2 = \beta^2 - k^2$ (β can be k_y or k_z) and $k = \omega\sqrt{\mu\varepsilon}$.

Setting $Z_{x>0}^{\mathrm{TM}}$ or $^{\mathrm{TE}} + Z_{x<0} = 0$ yields the following dispersion relations:

$$\frac{L\omega}{1 - LC\omega^2} = -\frac{u_2}{\omega\varepsilon}\tanh(u_2 b) \quad (\mathrm{TM}_x \text{ modes}) \tag{2a}$$

$$\frac{L\omega}{1 - LC\omega^2} = \frac{\omega\mu}{u_2}\tanh(u_2 b) \quad (\mathrm{TE}_x \text{ modes}). \tag{2b}$$

By replacing the equivalent L and C values of the EBG structures of Section II in (2a) and (2b), the dispersion diagrams presented in Fig. 6(a) for the three-layer EBG and in Fig. 7(a) for the two-layer EBG are obtained. In obtaining these diagrams, Fig. 7(b) is considered to be 1.54 mm and ε_r of the medium above the EBG is 4.

Since the equivalent *L–C* circuit incorporated in the TRM solution assumes a continuous surface, the accuracy of the result will decline as the wavelength becomes comparable with the periodicity of the structure. In the present TRM formulation, the wavenumber in the superstrate, i.e., u_2, is either purely imaginary or real. Therefore, for generality of the solution, this number should be considered complex. The left-hand sides of (2a) and (2b) present a reactive surface, which supports TM modes at frequencies below and TE modes at frequencies above the resonance. From Fig. 6(a) and 7(a), it is apparent that a bandgap is created between the first mode (TM_0), which starts as a TEM mode at dc and propagates as a surface wave afterwards, and the second mode, which is the TE_1 mode. The

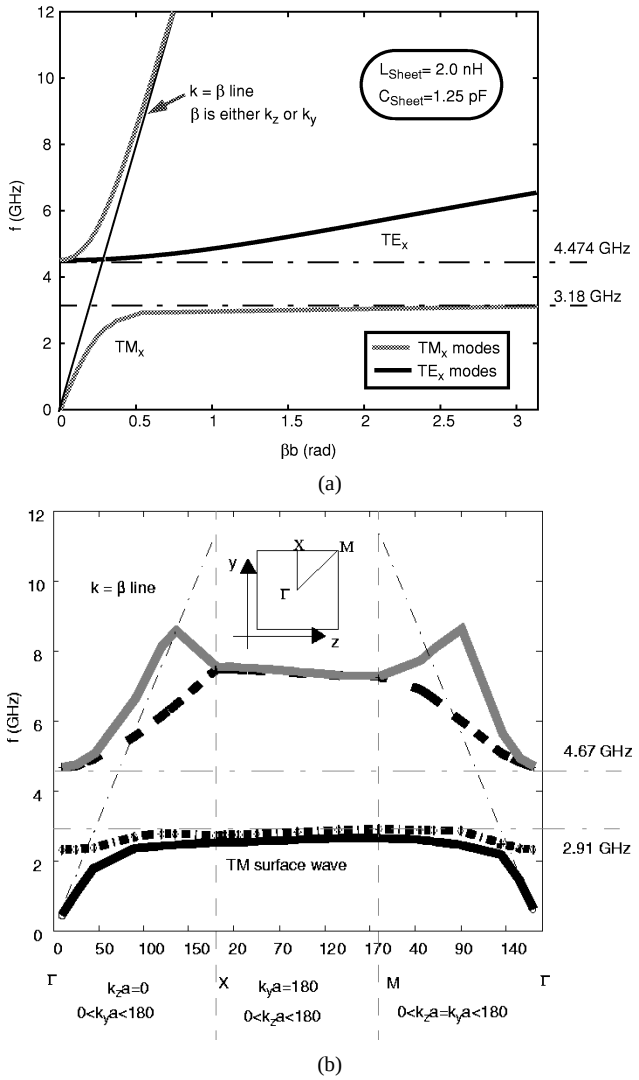

Fig. 6. Dispersion diagrams of the three-layer structure shown in Fig. 3(a). (a) TRM solutions. (b) FEM simulations.

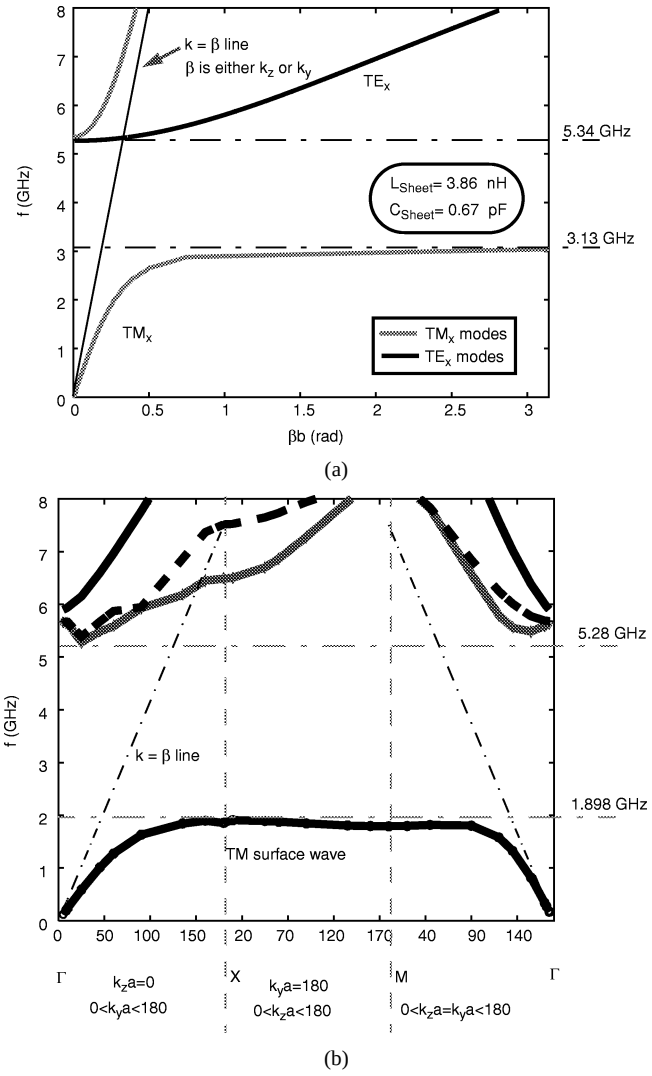

Fig. 7. Dispersion diagrams of the two-layer structure shown in Fig. 3(b). (a) TRM solutions. (b) FEM simulations.

bandgap for the three-layer structure is 1.294 GHz, ranging from 3.18 to 4.474 GHz, and for the two-layer structure is 2.21 GHz, residing from 3.13 to 5.34 GHz, as shown in Fig. 6(a) and 7(a), respectively.

Since the surface is modeled with only a single resonant circuit, this approach does not predict the cutoff frequency of the higher order modes. As well, no explicit information about the 2-D nature of the periodic structure and the direction of excitation, which is defined by the magnitude of the k_y and k_z components of the β vector, is included in this method. Therefore, a complete dispersion diagram for all possible directions of excitation cannot be generated.

B. Prediction of the Bandgap by Finite-Element Method (FEM) Simulations

In order to accurately predict the band structure for all the directions of excitation, a full-wave analysis is required. In a structure with 2-D periodicity in the y-z-plane, all directions can be covered by considering the k_y and k_z variable. Due to the symmetry of the unit cell, propagation through such a periodic structure contains redundant propagation vectors. Therefore, the unique propagation vectors can be grouped in a region called the irreducible Brillouin zone (reduced zone scheme) [13], [14], as shown by the $\Gamma\mathrm{XM}$ triangle in the inset of Fig. 6(b). In the dispersion diagram, different bands are all drawn in the first Brillouin zone and k_y and k_z are variables that trace the $\Gamma\mathrm{XM}$ triangle, i.e., the border of the irreducible zone. To this end, the unit cells of the PPW structures containing an EBG surface, as shown in Fig. 3(a) and (b), have been studied by means of eigenmode simulations for all the directions within the irreducable Brillouin zone with a commercial FEM CAD tool.

As shown in Fig. 6(b), for the three-layer structure, a bandgap of 1.76 GHz resides between the second and third modes with their corresponding cutoff frequencies of 2.91 and 4.67 GHz, respectively. The first and second modes, which have no H_x components, are clearly TM_x ones and coincide in most part of the dispersion diagram, except at low frequencies, where the first mode converges to a TEM pattern. It should be pointed out that, here, the type of a mode is determined by the field distribution in the superstrate, i.e., the volume between the top conductor plate and EBG surface, and in the $\Gamma - X$ region for $k_y a = 10^\circ$ and 135°. Due to the complexity of the three-layer

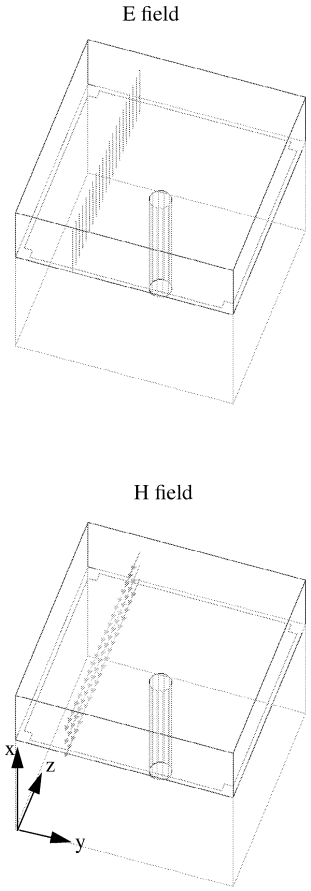

Fig. 8. E- and H-field profiles in the $\Gamma - X$ section of the dispersion diagram at $k_y a = 135^\circ$ for the first mode, which has a TM_x pattern.

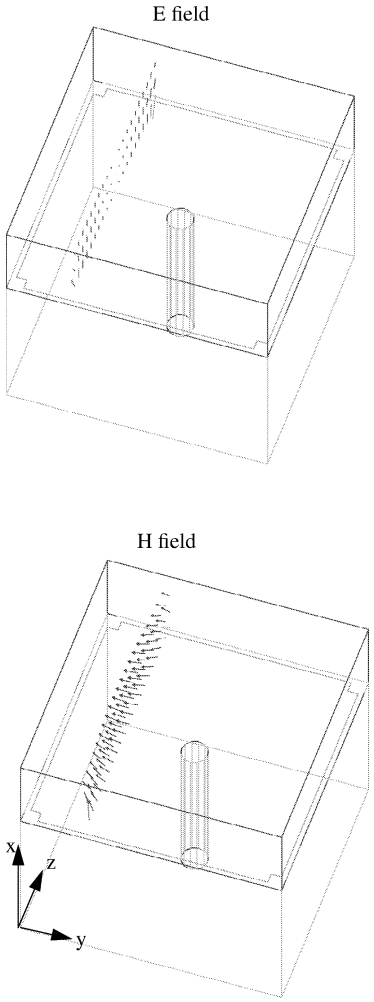

Fig. 9. E- and H-field profiles in the $\Gamma - X$ section of the dispersion diagram at $k_y a = 135^\circ$ for the second mode, which appears to be a hybrid mode.

structure, identifying the types of the third and fourth modes based on inspecting the field profile of a unit cell seems rather difficult since, at $k_y a = 10^\circ$, there is no H_x component, but at $k_y a = 135^\circ$, all the components of electric and magnetic fields exist.

Fig. 7(b) shows the dispersion diagram of the two-layer structure. A bandgap of 3.382 GHz exists between 1.898–5.28 GHz. Investigation of the field distributions at $k_y a = 10^\circ$ and 135° demonstrated that modes 1 and 4 have clearly TM_x-type field profile, however, the second and third modes exhibit hybrid mode patterns. The field profiles for the first and second modes in the $\Gamma - X$ region at $k_y a = 135^\circ$ are depicted in Figs. 8 and 9.

C. Measurement of the Stopband of the EBG Surface in a PPW Structure

To validate the simulation results in practice, four PPW structures have been fabricated. Two of these test-beds, shown in Fig. 10, are FR4-based PPW structures containing the fabricated EBG surfaces of Section II, and the other two (not shown) are their dual conventional PPWs (i.e., formed by using two solid metallic plates) with the same dielectric filling and port arrangement.

In Fig. 11(a), the insertion loss between Ports 1 and 2 of the test structure shown in Fig. 10(a) is presented. The EBG surface, around the resonance frequency, exhibits a very high impedance (open circuit), whereas at lower frequencies, behaves like a short

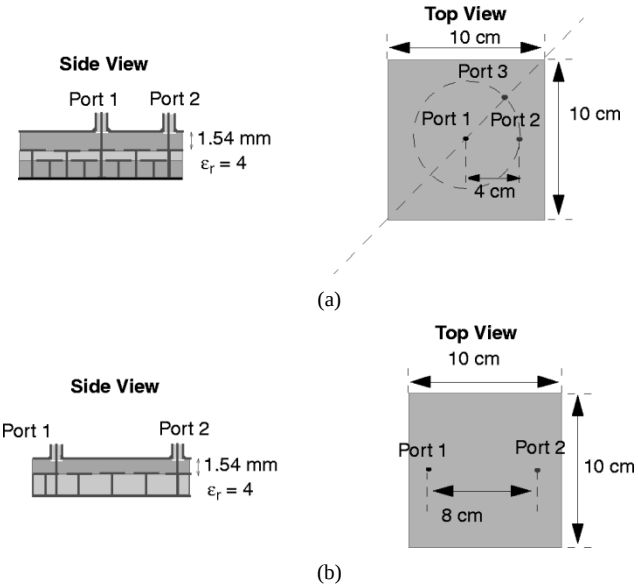

Fig. 10. Diagram of the fabricated PPW structures with EBG surfaces: (a) with the three-layer EBG and (b) with the two-layer EBG.

circuit, resembling a common parallel-plate environment. It can be observed that the obtained stopband, from 2.98 to 5.19 GHz,

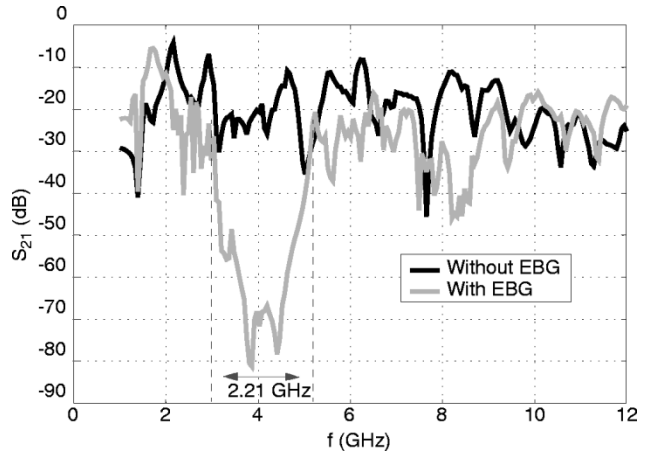

(a)

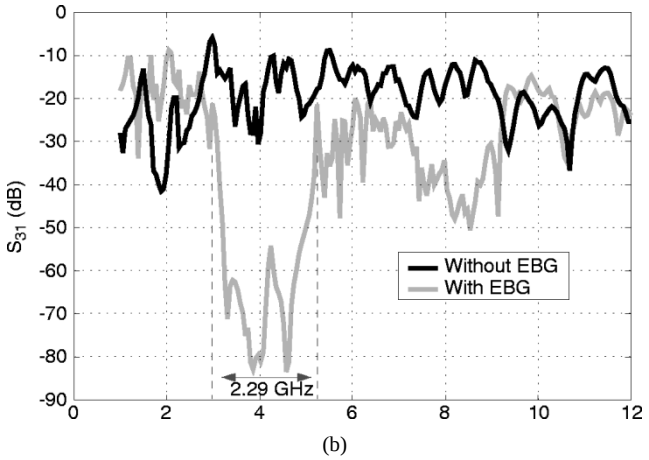

(b)

Fig. 11. Measured scattering parameters of the structure shown in Fig. 10(a). (a) S_{21}. (b) S_{31}.

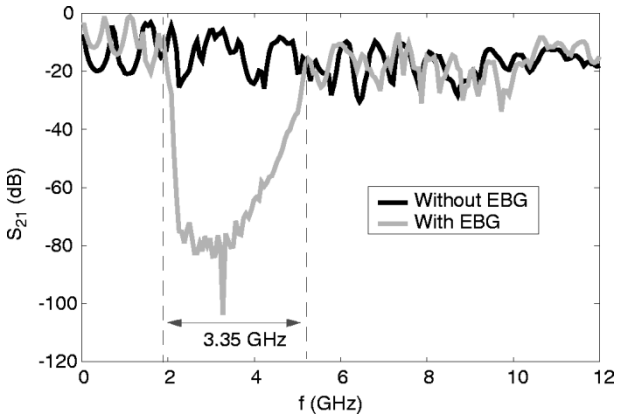

Fig. 12. Measured transmission coefficient S_{21} of the structure shown in Fig. 10(b).

TABLE I
PPW WITH THE THREE-LAYER EBG STRUCTURE

	TRM	FEM	S_{21} Measurements
fstart (GHz)	3.18	2.91	2.98
fstop (GHz)	4.474	4.67	5.19
Bandwidth (GHz)	1.294	1.76	2.21

TABLE II
PPW WITH THE TWO-LAYER EBG STRUCTURE

	TRM	FEM	S_{21} Measurements
fstart (GHz)	3.13	1.898	1.9
fstop (GHz)	5.34	5.28	5.25
Bandwidth (GHz)	2.21	3.382	3.35

corroborates the FEM simulation results of Fig. 6(b). To investigate the suppression of the noise in all directions, a via port was placed 4 cm away from the center of the board and at a 45° angle with respect to the line connecting Ports 1 and 2, as shown in Fig. 10(a). The measured S_{31}, which is presented in Fig. 11(b), corresponds to the bandgap along the $\Gamma - M$ direction in the dispersion diagram of Fig. 6(b). It can be seen that the stopband in the S_{31} measurement lies from 2.97 to 5.26 GHz, which is slightly wider than the stopband in the S_{21} measurement.

As expected, because of a higher *L/C* ratio, a wider bandgap was achieved when the scattering parameters of the test-bed shown in Fig. 10(b) were measured. In this structure, the spacing between Ports 1 and 2 is increased to 8 cm to contain eight periodic cells, as opposed to six in the three-layer structure. The measured S_{21}, as presented in Fig. 12, shows that a bandgap exists between 1.9–5.25 GHz, which corresponds well with the FEM results shown in Fig. 7(b). Note that the insertion loss in the stopband of Fig. 12 is higher than that of the S_{21} measurement shown in Fig. 11(a) due to the increased number of periodic cells.

In all the measurements discussed in this section and for all the PPW structures with and without EBG surfaces, the through via probes are solid wires that are soldered to the bottom conductor planes. Since the purpose of these measurement was validating the achievement of the predicted bandgaps, no impedance matching has been performed for the via probes to maximize the power transfer. This explains why S_{21} and S_{31} do not reach 0 dB in the passband regions presented in Figs. 11 and 12.

For comparison, all the results presented in Sections III-A–C are summarized in Tables I and II. The measurement and FEM simulation results match very well both for the three- and two-layer PPW structures. However, the TRM solutions, which employ the sheet impedance representation of the EBG surface, yield narrower bandgaps. On the other hand, the TRM approach has the least implementation cost of all of the three methods, while providing the fastest means of predicting a qualitative behavior of the dispersion characteristics. The errors in predicting the edges of the stopbands can be partly attributed to the approximate values considered for the sheet inductance and sheet capacitance. For instance, the inductance due to the via, which can acquire a significant value for long vias, is not included in the model. Therefore, the error in predicting the sheet inductance and, thus, the lower cutoff frequency of the bandgap (which is the resonance frequency of the *LC* circuit) from the TRM solutions is higher for the two-layer structure. By utilizing the closed-form expressions given in [15], values of 0.329 and 1.1 nH are calculated for the inductance of each via in the three- and two-layer EBG structures, respectively. As proposed in [10], the sheet inductance of the EBG surface is a result of the formation of a current loop in each cell of the periodic structure. This circulating current passes through at least two vias, therefore, the parasitic inductances due to the vias themselves should be included in the overall sheet inductance. The

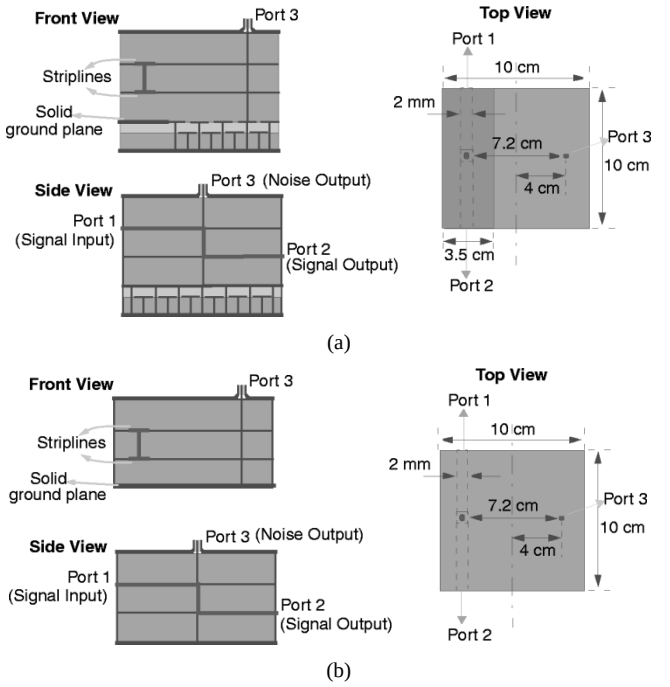

Fig. 13. (a) Stripline-via test-bed containing partial electric conductor and EBG planes. (b) The dual stripline-via structure with a solid ground plane.

corresponding adjusted sheet inductance is 6.06 nH/□ in the two-layer EBG structure. By recalculating the TRM solutions, a lower cutoff frequency of 2.5 GHz is obtained instead of the 3.13 GHz presented in Table II, which is closer to the measurement and full-wave simulation results. For the three-layer structure, the new adjusted sheet inductance is 2.658 nH/□, which yields 2.76 GHz as the lower cutoff frequency instead of the 3.18 GHz shown in Table I. As mentioned before, the sheet capacitance of the fabricated three-layer EBG is less than the calculated 1.25 pF·□ because of a thin layer of air existing between the two laminates, which results in a lower than expected resonance frequency. Note that the existence of the thin layer of air in this structure has been accounted for in the full-wave FEM simulations.

IV. Improved PPW Noise Isolation Results

To evaluate the idea of utilizing EBGs to suppress the parallel-plate noise, the test structure shown in Fig. 13, containing one through via and one buried via interconnecting two striplines, was fabricated. The stripline-via structure was placed closer to the left-hand side of the board and had a 3.5 cm $\times$10 cm solid conductor ground plane. The rest of the bottom surface, i.e., an area of 6.5 cm $\times$ 10 cm, was occupied by the three-layer EBG surface of Fig. 3(a). Furthermore, a through via was placed at the right-hand-side edge of the EBG ground to monitor the parallel-plate noise. Finally, several conducting strips were used to equalize the dc/low-frequency potential of the two planes. Similar to the measurement setup, reported in Section III-C, in order to scrutinize the performance of the structure shown in Fig. 13(a), an identical configuration with a complete (10 cm $\times$ 10 cm) conducting bottom ground plane [see Fig. 13(b)] was also fabricated and tested in both the time and frequency domains.

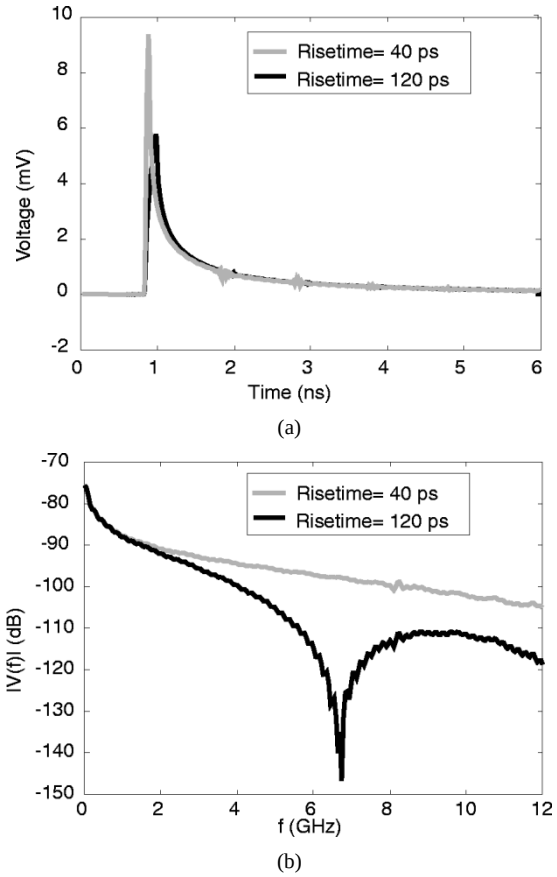

Fig. 14. Predicted PPW noise at Port 3 of the structure shown in Fig. 13(b) for two different rise times. (a) Time-domain signature. (b) Frequency-domain spectrum.

Following the same simulation approach as that of Section II, but here for the structure shown in Fig. 13(b), one can predict the noise waveform at Port 3 and inspect the effect of varying the rise time on the noise spectrum. As presented in Fig. 14(a), a stronger PPW noise is excited by decreasing the rise time of the input step at Port 1. From Fig. 14(b), it can be seen that the faster rise time (40 ps) creates a broader PPW noise bandwidth. Therefore, in a high-speed circuit, an EBG filter with a wider bandgap provides a more effective noise suppression. This notion is demonstrated in Section IV-B by employing the two fabricated EBG surfaces in the port isolation measurements.

A. S-Parameter Measurements

The scattering parameters of the three-port structure of Fig. 13(a) were measured and the magnitudes of S_{21} and S_{31} are plotted in Fig. 15. In this figure, the S-parameters of the corresponding structure with two complete grounds are also shown for comparison. It can be seen that the transmission coefficient S_{21} of the stripline-via structure of Fig. 13(a) has an identical signature as that of the stripline-via structure with the complete conducting planes of Fig. 13(b). However, the S_{31}-parameter, presented in Fig. 15(b), features a bandgap imposed by the EBG and, thus, exhibits an isolation of more than 45 dB over a 1-GHz bandwidth. The same level of isolation exists between Ports 2 and 3. These measurement results corroborate that, for the purpose of *isolating* a noisy ground

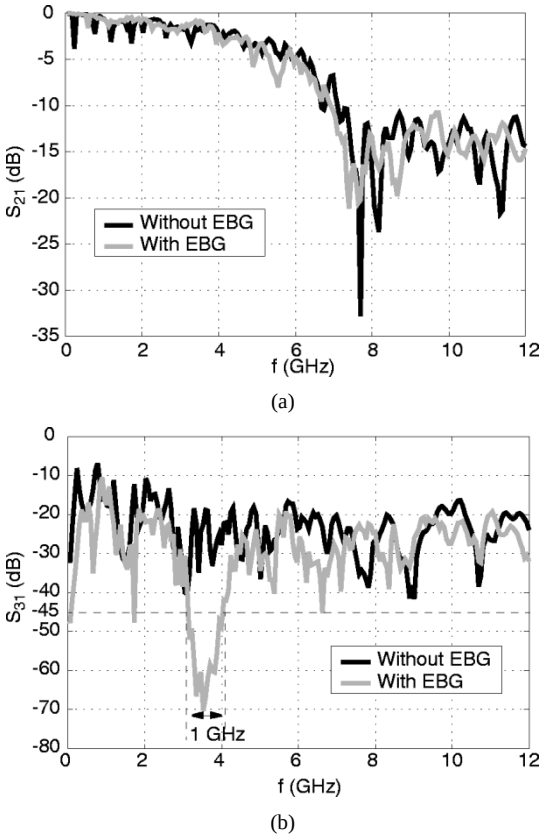

Fig. 15. Measured S-parameters of the two stripline-via structures shown in Fig. 13. (a) S_{21}. (b) S_{31}.

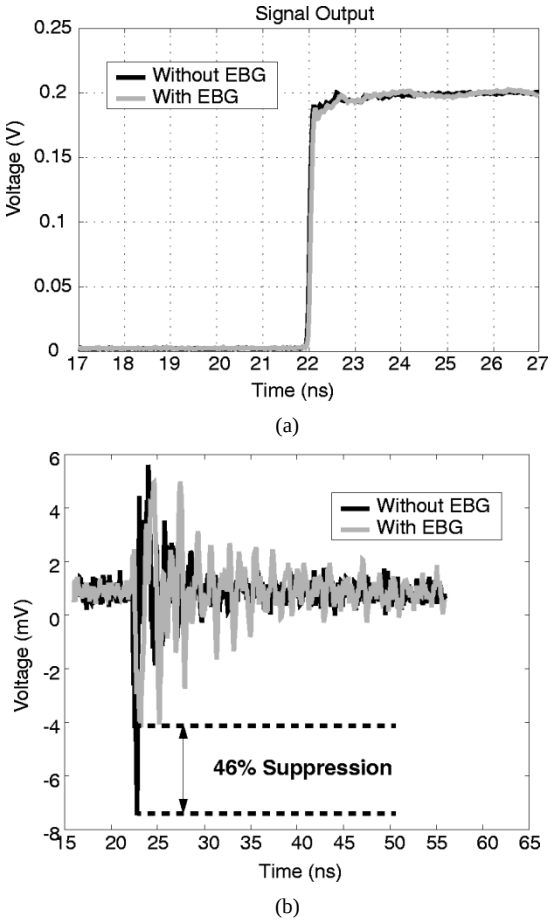

Fig. 16. TDR measurements of the two stripline-via structures shown in Fig. 13. (a) Output signals at Port 2. (b) Probed noise voltages at Port 3.

from the rest of the circuit, an efficient solution is to insert an EBG surface in the common ground.

B. TDR Measurements

Time-domain measurements were performed utilizing a TDR setup that generates a 200-mV step voltage. This signal is launched into the input ports (Port 1) of the stripline-via structures shown in Fig. 13. The transmitted signals to Port 2 of both test structures are shown in the same graph in Fig. 16(a), demonstrating almost identical output waveforms.

The most interesting result is obtained from the measurements of the PPW noise voltage at Port 3, as presented in Fig. 16(b). It is evident that, when the EBG ground is employed, the most prominent feature of the parallel-plate noise, i.e., the noise peak, is reduced by 46%. It should be mentioned here that, in [9], there has been an oversight in reporting the percentage of improvement, which instead should have been 46%. From Fig. 16(b), it can be seen that some reflections (resonance modes) appear to be enhanced by the presence of the EBG surface, but not exceeding the dominant noise peak. This phenomenon can be avoided by providing proper edge matching at the sidewalls of the PCB. This has been accounted for when the two-layer EBG of Section II was employed instead of the three-layer EBG, as shown in the inset of Fig. 17.

As well, in Fig. 17, the noise voltage detected at Port 3 of this structure is compared with the noise voltage at Port 3 of its dual PPW structure when similar edge matching is provided. Comparison of the two waveforms show a 53% reduction of the noise peak in the structure with EBG. It is important to point out

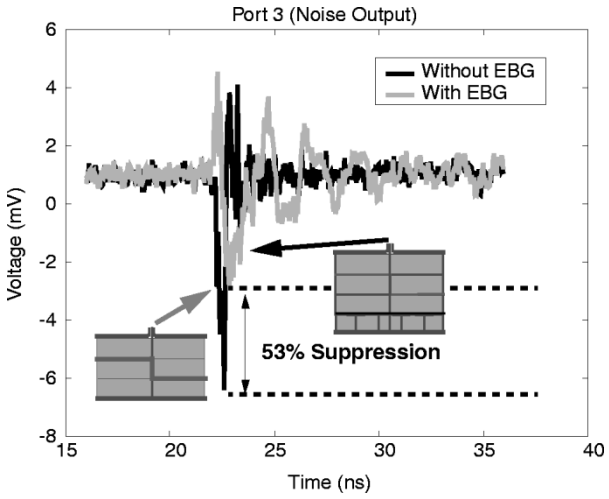

Fig. 17. Probed noise voltages from the TDR measurements of two stripline-via structures; one has the same partial ground configuration as the test-bed in Fig. 13(a) (but with the two-layer EBG surface instead of the three-layer one) and the other is the structure of Fig. 13(b).

that this drastic suppression of the parallel-plate noise occurs throughout the EBG surface and *in all azimuthal* directions, as opposed to other less efficient localized noise-suppression techniques. It should be mentioned that, even if the EBG surface replaces the entire bottom ground plane, with a careful choice of the design parameters, it is still possible to obtain an almost

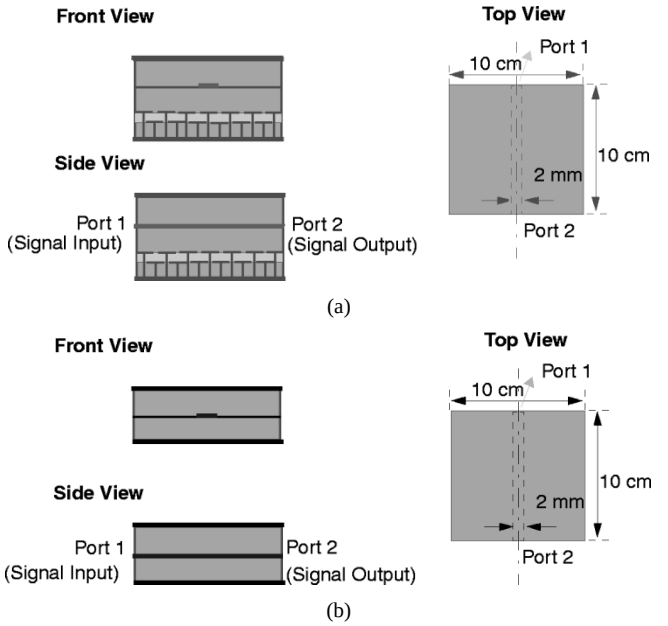

Fig. 18. (a) Stripline structure with a complete EBG ground plane. (b) The dual-stripline structure with two solid conductor grounds.

undistorted transmitted signal on the stripline while achieving an efficient global suppression of the parallel-plate noise. This aspect is further examined in Section V.

V. Signal Line Over an EBG Surface

In order to investigate the effect of the EBG surface on the signal, the performance of a stripline with and without the EBG ground plane has been investigated. To this end, two structures each containing a 2-mm-wide signal line, which is embedded midway in an FR4 substrate of 3.08-mm thickness, as shown in Fig. 18, have been fabricated. The structure of Fig. 18(a) incorporates the three-layer EBG surface of Fig. 3(a) as the bottom surface, and the structure shown in Fig. 18(b) is its dual conventional stripline configuration, where both top and bottom planes are solid conductors. The stripline of Fig. 18(b) has a characteristic impedance of 43.3 Ω. Therefore, the input signal, i.e., a 200-mV step with 110-ps rise time, will be partly reflected when launched into this line, as is shown in Fig. 19(a). However, when the EBG surface replaces the ground plane, due to the periodic loading of the line, the characteristic impedance varies from 46.08 to 53.92 Ω, which is close to the reference 50-Ω impedance and provides a better matching.

The output signals at Port 2 for both structures are presented in Fig. 19(b). As shown, an overshoot of 5% appears in the output signal of the structure with the EBG ground, which is within the overshoot tolerance range of most logic families [16].

The S_{21}-parameter has also been measured to assess the effect of the bandgap on the transmission of the signals on the striplines. It can be observed from the frequency-domain measurements of Fig. 20 that a stopband with approximately 6-dB maximum attenuation occurs within the 2.4–3.3-GHz band, which is slightly off, but mostly within the measured bandgap range of Section III. It was also observed from further measurements that, at frequencies beyond 6.2 GHz, the enhanced resonances due to the presence of the EBG surface

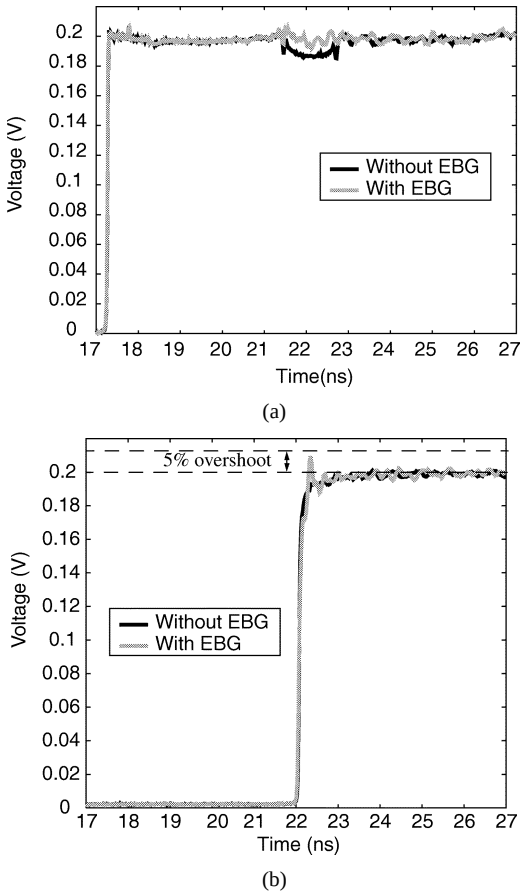

Fig. 19. TDR measurements of the stripline structure shown in Fig. 18. (a) Input port. (b) Output port.

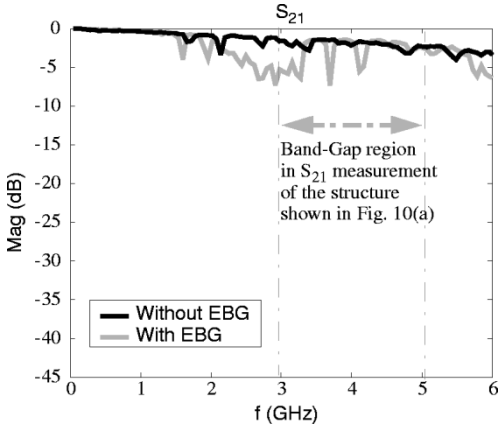

Fig. 20. Measured S_{21} of the structures shown in Fig. 15.

cause a higher transmission loss, which implies more distortion for signals with rise times faster than 110 ps.

VI. Conclusions

A novel approach for the suppression of the parallel-plate noise in high-speed circuits has been proposed. Specifically, a metallo-dielectric EBG surface is proposed to replace one of the electric conductor ground planes in parallel-plate structures containing vias. This EBG structure is realizable at low frequencies (< 6 GHz), but nevertheless leads to compact structures. Since the EBG surface contains no slots, it offers immunity to

parasitic radiation and power leakage. Unlike traditional *localized* noise-suppression methods, this proposed technique offers the ability to suppress the PPW noise *globally* over the entire substrate

To validate the concept, a number of test structures were designed and fabricated. A simple recursive algorithm for the design of an EBG filter has been proposed. The bandgap of a PPW formed with one solid conductor and one EBG surface has been predicted through fast analytical TRM solutions and has been validated with more accurate full-wave FEM simulations. Measurements on the PPW structures containing different EBG surfaces demonstrated achievement of wide stopbands (2.21 and 3.35 GHz) at the low gigahertz frequency range. Port isolation experiments have proven the efficiency of the approach for the purpose of segregating a noisy ground in a high-speed circuit by the achievement of 53% reduction of the PPW noise peak. As well, it was demonstrated that, with a careful choice of the design parameters, a stripline running above an EBG surface is capable of supporting an almost undistorted transmitted signal while maintaining an efficient global suppression of the parallel-plate noise.

REFERENCES

[1] R. Abhari, G. V. Eleftheriades, and T. E. van Deventer-Perkins, "Physics-based CAD models for analysis of vias in parallel-plate environments," *IEEE Trans. Microwave Theory Tech.*, vol. 49, pp. 1697–1707, Oct. 2001.

[2] M. I. Montrose, *EMC and the Printed Circuit Board Design, Theory and Layout Made Simple*. Piscataway, NJ: IEEE Press, 1999.

[3] A. Madou and L. Martens, "Electrical behavior of decoupling capacitors embedded in multilayered PCBs," *IEEE Trans. Electromagn. Compat.*, vol. 43, pp. 549–556, Nov. 2001.

[4] G.-T. Lei, R. W. Techentin, and B. K. Gilbert, "High-frequency characterization of power/ground-plane structures," *IEEE Trans. Microwave Theory Tech.*, vol. 47, pp. 562–569, May 1999.

[5] R. Abhari, G. V. Eleftheriades, and T. E. van Deventer-Perkins, "Analysis of differential vias in multilayer parallel plate environment using a physics-based CAD model," in *IEEE MTT-S Int. Microwave Symp. Dig.*, May 2001, pp. 2031–2034.

[6] K.-P. Ma, J. Kim, F.-R. Yang, Y. Qian, and T. Itoh, "Leakage suppression in stripline circuits using a 2-D photonic bandgap lattice," in *IEEE MTT-S Int. Microwave Symp. Dig.*, June 1999, pp. 73–76.

[7] D. Sievenpiper, L. Zhang, R. F. J. Broas, N. G. Alexopolous, and E. Yablonovitch, "High- impedance electromagnetic surfaces with a forbidden frequency band," *IEEE Trans. Microwave Theory Tech.*, vol. 47, pp. 2059–2074, Nov. 1999.

[8] N. Shino and Z. Popović, "Radiation from ground-plane photonic bandgap microstrip waveguide," in *IEEE MTT-S Int. Microwave Symp. Dig.*, June 2002, pp. 1079–1082.

[9] R. Abhari and G. V. Eleftheriades, "Suppression of the parallel-plate noise in high-speed circuits using a metallic electromagnetics band-gap structure," in *IEEE MTT-S Int. Microwave Symp. Dig.*, June 2002, pp. 493–496.

[10] D. Sievenpiper, "High-impedance electromagnetic surfaces," Ph.D. dissertation, Dept. Elect. Eng., UCLA, Los Angeles, CA, 1999.

[11] Y.-J. Park, A. Herschlein, and W. Wiesbeck, "A photonic bandgap (PBG) structure for guiding and suppressing surface waves in millimeter-wave antennas," *IEEE Trans. Microwave Theory Tech.*, vol. 49, pp. 1854–1859, Oct. 2001.

[12] R. F. Harrington, *Time–Harmonic Electromagnetic Fields*. New York: McGraw-Hill, 1961, pp. 208–212.

[13] L. Brillouin, *Wave Propagation in Periodic Structures; Electric Filters and Crystal Lattices*. New York: McGraw-Hill, 1946.

[14] C. Kittel, *Introduction to Solid State Physics*. New York: Wiley, 1996.

[15] F. W. Grover, *Inductance Calculations: Working Formulas and Tables*. New York: Dover, 1962.

[16] B. Young, *Digital Signal Integrity: Modeling and Simulations With Interconnects and Packages*. Upper Saddle River, NJ: Prentice-Hall, 2001.

Ramesh Abhari (S'97) received the B.A.Sc. degree in electrical engineering from Tehran Polytechnique, Tehran, Iran, in 1992, the M.A.Sc. degree in electrical engineering from the Iran University of Science and Technology, Tehran, Iran, in 1996, and is currently working toward the Ph.D. degree in electrical and computer engineering at the University of Toronto, Toronto, ON, Canada.

From September 1996 to September 1997, she was a Research Associate with the Electromagnetics Group, University of Toronto, where she was involved with projects supported by Nortel Networks, Canada. Her current research interests include analysis and modeling of high-speed interconnects, microwave and millimeter-wave circuits, EBG structures, signal integrity, and suppression of the power/ground noise.

Ms. Abhari has been the chairperson of the IEEE Toronto Section Electromagnetics and Radiation Chapter (IEEE Microwave Theory and Techniques (MTT)/Antennas and Propagation (AP)/Electromagnetic Compatibility (EMC) Societies) since 1998. She was the recipient of the 2000 IEEE Microwave Theory and Techniques Society (IEEE MTT-S) Graduate Fellowship and the Third Place Student Paper Award presented at the 2002 IEEE MTT-S International Microwaves Symposium (IMS), Seattle, WA.

George V. Eleftheriades (S'86–M'88–SM'02) received the Diploma (with distinction) in electrical engineering from the National Technical University of Athens, Athens, Greece in 1988, and the Ph.D. and M.S.E.E. degrees in electrical engineering from The University of Michigan at Ann Arbor, in 1993 and 1989, respectively.

From 1994 to 1997, he was with the Swiss Federal Institute of Technology, Lausanne, Switzerland, where he was engaged in the design of millimeter and sub-millimeter-wave receivers and in the creation of fast computer-aided design (CAD) tools for planar packaged microwave circuits. He is currently an Associate Professor with the Department of Electrical and Computer Engineering, University of Toronto, Toronto, ON, Canada. He has authored or coauthored over 80 papers in refereed journals and conference proceedings. His current research interests include negative refractive index metamaterials, integrated circuit (IC) antennas and components for broad-band wireless communications, novel beam-steering techniques, low-loss silicon micromachined components, millimeter-wave radiometric receivers, and electromagnetic design for high-speed digital circuits.

Dr. Eleftheriades was a corecipient of the 1990 Best Paper Award presented at the 6th International Symposium on Antennas (JINA) and the Ontario Premier's 2001 Research Excellence Award. His graduate students were the recipients of Student Paper Awards presented at the 2000 Antenna Technology and Applied Electromagnetics Symposium, the 2002 IEEE Microwave Theory and Techniques Society (IEEE MTT-S) International Microwave Symposium (IMS), and the 2002 IEEE International Symposium on Antennas and Propagation.